ACS APPLIED MATERIALS & INTERFACES

Research Article

www.acsami.org

Monitoring Thrombin Generation and Screening Anticoagulants through Pulse Laser-Induced Fragmentation of Biofunctional Nanogold on Cellulose Membranes

Yu-Jia Li,[†] Wei-Jane Chiu,[†] Binesh Unnikrishnan,[†] and Chih-Ching Huang*[,†,‡,§]

[†]Institute of Bioscience and Biotechnology, National Taiwan Ocean University, Keelung 20224, Taiwan

[‡]Center of Excellence for the Oceans, National Taiwan Ocean University, Keelung 20224, Taiwan

[§]School of Pharmacy, College of Pharmacy, Kaohsiung Medical University, Kaohsiung 80708, Taiwan

Supporting Information

ABSTRACT: Thrombin generation (TG) has an important part in the blood coagulation system, and monitoring TG is useful for diagnosing various health issues related to hypo-coagulability and hyper-coagulability. In this study, we constructed probes by using mixed cellulose ester membranes (MCEMs) modified with gold nanoparticles (Au NPs) for monitoring thrombin activity using laser desorption/ionization mass spectrometry (LDI–MS). The LDI process produced Au cationic clusters ($[Au_n]^+$; n = 1–3) that we detected through MS. When thrombin reacted with fibrinogen on the Au NPs–MCEMs, insoluble fibrin was formed, hindering the formation of Au cationic clusters and, thereby, decreasing the intensity of their signals in the mass spectrum. Accordingly, we incorporated fibrinogen onto the Au NPs–MCEMs to form Fib–Au NPs–MCEM probes to monitor TG with good selectivity (>1000-fold toward thrombin with respect to other proteins or enzymes) and sensitivity (limit of detection for thrombin of ca. 2.5 pM in human plasma samples). Our probe exhibited remarkable performance in monitoring the inhibition of thrombin activity by direct thrombin inhibitors. Analyses of real samples using our new membrane-based probe suggested that it will be highly useful in practical applications for the effective management of hemostatic complications.

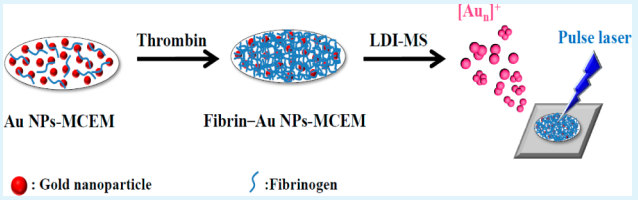

KEYWORDS: *thrombin generation, drugs screening, gold nanoparticles, cellulose membranes, laser desorption/ionization*

INTRODUCTION

Pulse lasers are very powerful and useful tools in modern nanoscience and nanotechnology.[1−3] Lasers can provide high photon densities, a variety of photon energies, and pulse widths ranging in duration from femto- to nanoseconds to permit controlled excitation.[4] Lasers have been used for manipulation of substrates at nanoscale levels and for optical pumping applications of nanoscopic structures.[1−3,5,6] In addition, laser treatment can be used very successfully for preparing nanoparticles (NPs) of various sizes, shapes, and chemical compositions, and therefore, various optical, electromagnetic, and chemical properties.[7,8] Accordingly, pulse lasers are innovative tools in the field of nanoscopic processing. Two effects have been identified in the pulse laser irradiation of metallic NPs at various laser intensities, wavelengths, and pulse durations: fusion and fragmentation.[4,9,10] The fragmentation of metallic NPs under pulse laser illumination has been explained by photothermal evaporation and coulomb explosion mechanisms.[3,11,12] In the photothermal mechanism, absorption of laser energy by an NP leads to thermal heating, followed by surface melting and an eventual decrease in size, due to evaporation from the entire particle, especially from its surface.[3,11−14] According to this model, the degree of surface evaporation depends on the thermal energy transfer to the lattice system that results in the heating of NPs to their evaporation point. The evaporation point depends on the evaporation pressure of the material. Conversely, according to the coulomb explosion mechanism, the explosion occurs due to the ejection of large number of electrons that generates multiply ionized NPs (through thermoionic emission and/or photoionization) and they undergo spontaneous fission as a result of charge repulsion.[3,15−17] The pulse laser-induced fragmentation of metallic NPs results in the formation of a large number of tiny NPs or cluster ions.[3,11−17] On the other hand, control over the irradiation intensity and pulse duration can also induce fusion of most NPs, through thermal or nonthermal melting and surface welding.[18]

Owing to their interesting optical and electronic properties, Au NPs are most widely used for fabricating miniaturized optical devices, photonic circuits, and sensors and for use in cell labeling.[19−21] The UV–visible absorption characteristics of Au NPs are determined by both inter- and intraband transitions.[22,23] Intraband excitation of free conduction electrons on the surfaces of Au NPs results in surface plasmon absorptions

Received: June 8, 2014
Accepted: August 20, 2014
Published: August 20, 2014

 © 2014 American Chemical Society

Scheme 1. Schematic Representation of the Preparation of a Au NPs−MCEM and Its Use in Conjunction with Laser Desorption/Ionization Mass Spectrometry (LDI−MS) for the Analysis of Thrombin

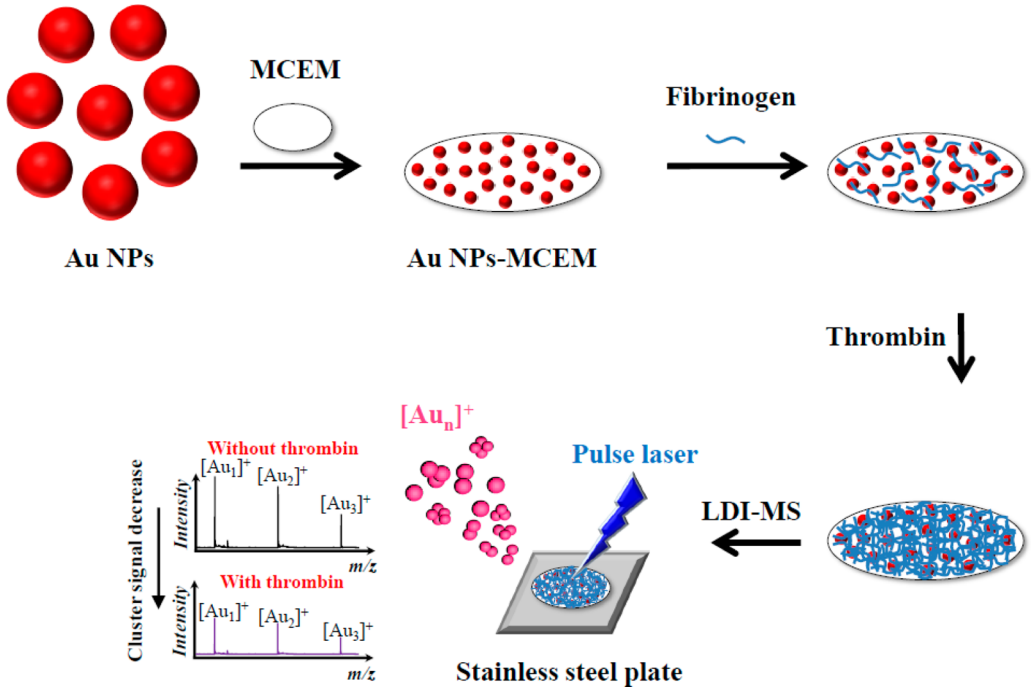

near 520 nm with extremely high absorption coefficients (10^8–10^{10} M^{-1} cm^{-1}). The position of the peak in the spectrum and the absorption coefficient of the Au NPs depend mainly on the size and shape of the NPs as well as their interparticle distances.[24,25] In contrast, interband transitions contribute mainly to absorptions at wavelengths of less than 400 nm.[26,27] The spectral feature of the interband transition does not change significantly upon varying the diameter of the Au NPs because it relates to the response of their d electrons. The nanosecond transient absorption of Au NPs under excitation by a pulse laser (Nd:YAG) at 532 or 355 nm leads to the formation of multiply ionized Au NPs.[28,29] The ionization efficiency is highest when the interband transition of the Au NPs is resonantly excited (excited by 355 nm laser); in contrast, intraband excitation (532 nm laser) hardly contributes to the ionization process. In principle, during the period of the laser pulse, multiply charged Au NPs could dissociate into smaller ones, with these as-produced small NPs or cluster ions further absorbing photons to reach highly charged states.[30] Although analyses of cluster ions can provide insight into the ionization mechanisms of metallic NPs, related studies and applications are rare. The formation of Au cluster ions from Au NPs under pulse laser irradiation is very sensitive to the laser intensity and the particles' sizes and surface properties; for example, our earlier studies showed that the efficiency of the formation of Au cluster ions from Au NPs decreases in the presence of thiolated-DNA.[31] Through analyses of Au and/or Au-hybrid cluster ions formed from functional Au NPs through nanosecond pulse laser irradiation, it is possible to selectively detect heavy metal ions, anions, DNA, and proteins, as well as bacteria.[31−33] Also, functionalized Au NPs can be employed to selectively enrich biomolecules such as glycopeptides and glycoproteins.[34,35]

In this work, we demonstrated an LDI−MS based approach for monitoring thrombin generation and screening anticoagulants in human plasma by using functional nanogold-adsorbed mixed cellulose ester membrane (Au NPs−MCEM). First, we fabricated a functional membrane substrate by modification with fibrinogen (Fib) on Au NPs−MCEM. We employed this system for monitoring thrombin activity by measuring the Au cluster ions signal, which is negatively influenced by the concentration of thrombin and its activity on converting soluble fibrinogen to insoluble fibrin structures on the MCEM (Scheme 1). Thrombin has an imperative role in the coagulation cascade and it converts soluble fibrinogen into insoluble fibrin. Moreover, it also catalyzes many other coagulation-related reactions.[36,37] Thrombin-generation (TG) assays generally determine the active thrombin concentration that is produced in plasma after activation of coagulation with tissue factor or another trigger.[38−40] TG tests can evaluate the overall coagulation function and, thereby, reliably estimate the bleeding and thrombosis risk in each individual patient. A number of TG assays have been developed involving fluorogenic or chromogenic substrates.[38−40] However, these methods have limitations such as using expensive synthetic compounds, low affinity toward thrombin, low converted rate, and tedious labeling and sample preparation.

Our new Fib−Au NPs−MCEM/LDI−MS sensing system provides very clean mass spectra, allowing monitoring of Au cluster ions under pulse laser desorption/ionization process. We studied the influence of Au NP's size and laser intensity on the formation of these Au cluster ions. Because of the homogeneous deposition of Au NPs on the MCEM, the Fib−Au NPs−MCEM nanocomposite provided excellent shot-to-shot reproducibility for the detection of thrombin. The Fib−Au NPs−MCEM/LDI−MS probe displayed high selectivity for the detection of thrombin, and we were able to apply this system to monitor thrombin generation induced by Factor Xa in human plasma and in the screening of inhibiting drugs of thrombin.

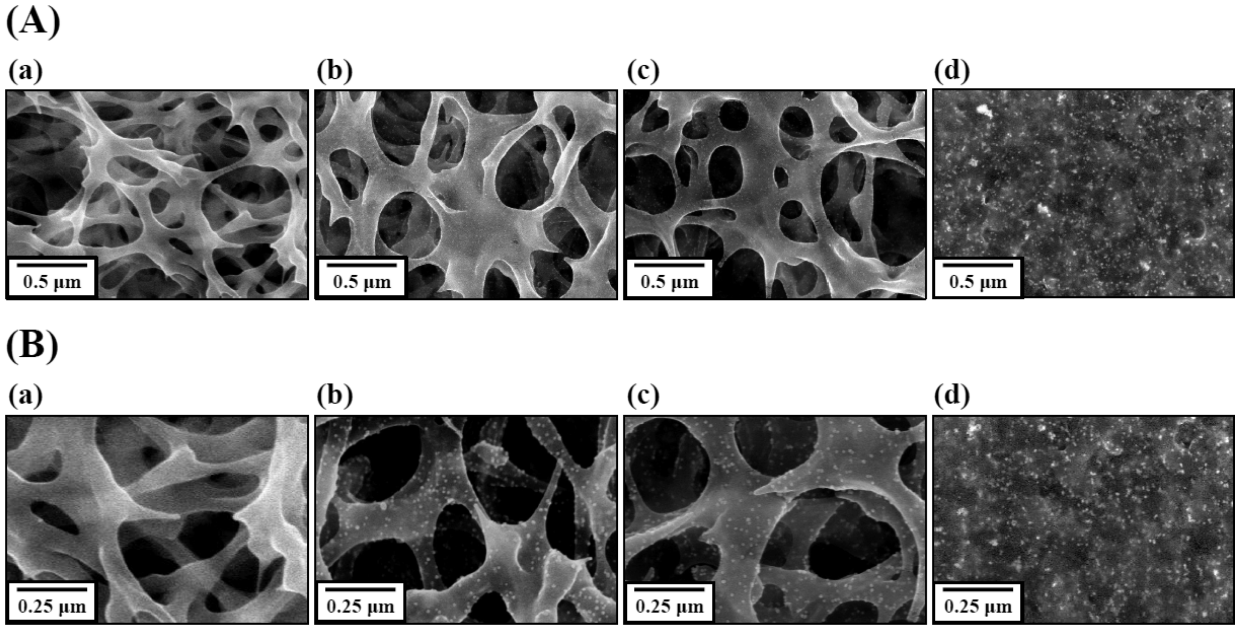

Figure 1. (A) Low- and (B) high-magnification SEM images of (a) an MCEM, (b) a Au NPs−MCEM, (c) a Au NPs−MCEM in the presence of fibrinogen (1.0 μM), and (d) a Au NPs−MCEM in the presence of fibrinogen (1.0 μM) and thrombin (100 pM). The catalytic reaction of thrombin and fibrinogen was conducted in PBS for 1 h.

MATERIALS AND METHODS

Chemicals and Materials. Tris(hydroxymethyl)aminomethane (Tris), calcium chloride, potassium chloride, hydrochloric acid, magnesium chloride and sodium chloride were obtained from Mallinckrodt Baker (Phillipsburg, NJ). Trisodium citrate was obtained from Aldrich (Milwaukee, WI). Hydrogen tetrachloroaurate(III) trihydrate was obtained from Acros (Geel, Belgium). α-Thrombin (human, ≥1000 NIH units/mg protein; NIH units obtained by direct comparison to a NIH Thrombin Reference Standard),[41] Factor Xa (human), fibrinogen (human), hemoglobin (human), α-lactalbumin (bovine milk), lysozyme (chicken egg white), conalbumin (chicken egg white), β-lactoglobulin (bovine milk), lipase (porcine pancreas), phosphatase alkaline (bovine intestinal mucosa), trypsin (bovine pancreas), human serum albumin, transferrin (human), and bovine serum albumin (BSA) were obtained from Sigma (St. Louis, MO). The MCEM (pore size, 0.45 μm; thickness, 145 μm; porosity, 75%) was purchased from GE Healthcare Bioscience (Buckinghamshire, U.K.). A 5 mM Tris−HCl buffer solution (pH 7.4) containing 150 mM NaCl, 5 mM KCl, 1 mM $MgCl_2$, and 1 mM $CaCl_2$ was used to mimic physiological conditions. Milli-Q ultrapure water (Millipore, Billerica, MA) was used in all experiments.

Preparation of Au NPs−MCEM. Au NPs having various sizes of 13, 32, and 56 nm were prepared following a procedure reported elsewhere with slight modification.[42] The particle concentrations of the 13, 32, and 56 nm Au NPs were 15 nM, 280 pM, and 54 pM, respectively.[43] Forty MCEMs (diameter: 0.6 cm) were immersed in Au NP solution (20 mL) in 2.5 mM citrate (pH 5.8) in a 20 mL vial and incubated for 2 h. Each Au NPs-modified MCEM was gently washed with 20 mL of deionized water for 30 s and dried in air for 1 h. Color analysis of each prepared membrane was conducted by scanning using a desktop scanner (Epson Perfection 1660 Photo Scanner). The color intensity of the pixels of the scanned image (red, green, and blue) was measured by using the ImageJ computer program (National Institutes of Health, Bethesda, MD).

Detection of Thrombin by LDI−MS Using Au NPs−MCEM as Substrate. As-prepared Au NPs−MCEMs were immersed in aliquots (1.0 mL) of physiological-mimicking buffer solution [PBS; 5 mM Tris−HCl buffer (pH 7.4) containing 150 mM NaCl, 5 mM KCl, 1 mM $MgCl_2$, and 1 mM $CaCl_2$] containing BSA (100 μM), fibrinogen (1.0 μM), and thrombin (0−1.0 nM) and equilibrated for 1 h at room temperature. The membranes were gently washed with deionized water (5 mL) for 30 s, dried for 1 min using an air gun (60 lb in.$^{-2}$), and then attached to a laser desorption/ionization (LDI) plate using an adhesive polyimide film tape.[32] When thrombin interacts with the fibrinogen immobilized on the Au NPs−MCEMs, it causes the polymerization of the later to form a fibrous and nonglobular protein, fibrin. Fibrins are long strands of insoluble proteins which are highly adsorbed to the Au NPs−MCEMs and are not easily removed during washing with DI water. MS experiments were conducted by using an AutoflexIII LDI time-of-flight (TOF) mass spectrometer (Bruker Daltonics, Bremen, Germany). The MS instrument was set in the reflectron positive-ion mode with a delayed extraction period of 20 ns to stabilize the positive ions generated in the LDI process. A total of 300 pulsed laser shots (355 nm Nd:YAG, 100 Hz, pulse width: 6 ns) with a laser fluence of 5.57×10^4 W cm^{-2} were used for the irraditiaon of samples at five random positions on the MALDI taget plate. The positive ions were then accelerated through the TOF chamber.

Analysis of Thrombin and Factor Xa in Plasma Samples. To obtain plasma samples, the blood was collected in tubes containing ethylenediaminetetraacetic acid (EDTA), centrifuged at 3000*g* for 10 min at 4 °C, and stored at −80 °C until required for analysis. One milliliter of 10-fold-diluted plasma samples was then spiked with various concentrations of thrombin (0−10 nM) solutions containing a Au NPs−MCEM in PBS solution in the presence of BSA (100 μM) and fibrinogen (1.0 μM) and incubated for 1 h. The Au NPs−MCEM substrate was gently washed with DI water (5 mL) for 30 s and then dried for 1 min using an air gun (60 lb in.$^{-2}$). This substrate was attached to a LDI plate using an adhesive polyimide film tape prior to LDI−MS measurement.[33]

For monitoring Factor Xa in plasma samples, Au NPs−MCEMs were equilibrated with a series of 200-fold diluted plasma, 1.0 μM fibrinogen and 50 μM phospholipids in PBS solution at room temperature for 10 min. Then, aliquots of Factor Xa with different concentrations were spiked into the mixtures to obtain final concentrations from 0 to 10 pM and the samples were kept for 2 h to attain equilibrium. Then, the membranes were washed, dried, and sent for LDI−MS measurement with the same procedure mentioned above for monitoring thrombin generation.

Assays of Anticoagulant Drugs. To screen anticoagulant drugs, aliquots (500 μL) of PBS solution (pH 7.4) containing BSA (200 μM), and fibrinogen (2.0 μM) were maintained at room temperature. The Au NPs−MCEMs were immersed in the resulting solution at

room temperature and kept for 10 min. Finally, anticoagulant drug (100 nM or 1.0 μM) and thrombin (1.0 nM) were mixed in PBS (500 μL) and the mixture was maintained at room temperature for 30 min and then mixed with the solutions. After reacting for 1 h of incubation, the Au NPs–MCEMs were taken out, gently washed, and dried and sent for LDI–MS measurement with the same proceedure mentioned above for monitoring thrombin generation.

RESULTS AND DISCUSSION

Analysis of Thrombin-Induced Formation of Fibrin. Scheme 1 depicts the preparation of Au NPs–MCEMs, through simple electrostatic and interfacial interactions between cellulose units (cellulose nitrate and cellulose acetate) and Au NPs, and their application for monitoring thrombin activity using LDI–MS. The desorption of Au NPs from the MCEM was less than 3% after we had incubated the Au NPs–MCEMs in phosphate buffered saline [5 mM Tris–HCl buffer solution (pH 7.4) containing 150 mM NaCl, 5 mM KCl, 1 mM $MgCl_2$, and 1 mM $CaCl_2$] for 48 h. Figure 1 and Figure S1A (Supporting Information) reveal homogeneous distribution of 13 nm Au NPs on the MCEM as well as interior of the porous structures of MCEM (ca. 400 nm) during the incubation period. The smartbeam laser irradiation (355 nm Nd:YAG; pulse width, 6 ns; 5.57×10^4 W cm^{-2}; beam diameter, ca. 5 μm), caused photoabsorption, and desorption and ionization of surface atoms from the 13 nm Au NPs. Signals for cationic clusters ($[Au_n]^+$; n = 1–3) were dominant in the mass spectra

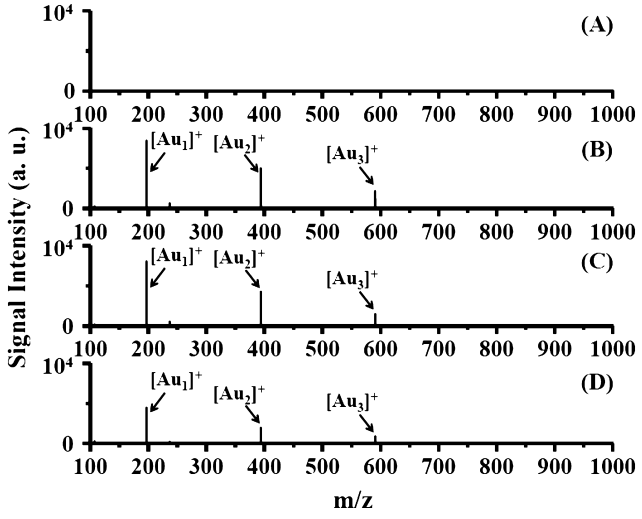

Figure 2. LDI mass spectra of (A) an MCEM, (B) a Au NPs–MCEM, (C) a Au NPs–MCEM in the presence of fibrinogen (1.0 μM), and (D) a Au NPs–MCEM in the presence of fibrinogen (1.0 μM) and thrombin (100 pM). The peaks at m/z 196.97, 393.93, and 590.90 are assigned to the ions $[Au_1]^+$, $[Au_2]^+$, and $[Au_3]^+$, respectively. A total of 300 pulsed laser shots at a laser density of 5.57×10^4 W cm^{-2} were applied to five random positions on the MALDI target. Peak intensities are plotted in arbitrary units (au).

(Figure 2B). Au NPs absorb energy (E_{abs}) from an individual pulse of laser light according to eq 1.[44]

$$E_{abs} = (E_0/S_0) \times \sigma_{abs}^{\lambda} \quad (1)$$

where E_0 is the pulse energy, S_0 is the beam cross section, and σ_{λ}^{abs} is the particle absorption cross section. For a spherical NP, the relative absorption cross section is also known as the absorption efficiency (Q_{λ}^{abs}), which can be calculated using eq 2

$$Q_{abs}^{\lambda} = (4 \times \sigma_{abs}^{\lambda})/(\pi \times d_p^2) \quad (2)$$

where $\pi \times d_p^2/4$ is the particle geometrical cross section.[44] Both Q and σ are dependent on the wavelength (λ). Moreover, the formation yield (Y_n) of a metallic cluster of n atoms/ions is proportional to $n^{-\delta}$, where δ is related to the total sputter yield.[43,45] As a result, the signal intensity of $[Au_1]^+$ ions was much higher than that of $[Au_2]^+$ and $[Au_3]^+$ cluster ions (Figure 2B). The Au NPs–MCEMs presumably provided such clean mass spectra because the negatively charged sites of the MCEM effectively bound the cationic molecules and thus limit or eliminate interference during the LDI process. Thus, the relative standard deviations (RSDs) of these Au cluster ions signals ($[Au_1]^+$, $[Au_2]^+$, ($[Au_3]^+$) were all less than 10%, insinuating that the Au NPs were not aggregated—but, rather, adsorbed homogeneously—on the MCEMs (Figure 1B). In contrast to the Gaussian beam profile of a standard Nd:YAG laser, the near-flat top energy profile of the "smartbeam" laser-induced the desorption/ionization of Au NPs on the homogeneous porous MCEMs—another likely contributor to the excellent reproducibility in obtaining Au ions signals.[46]

The peak intensities of the $[Au_n]^+$ cluster ions in the absence and presence of fibrinogen (1.0 μM) did not show any difference (Figure 2B,C). After the addition of 100 pM thrombin (Figure 2D), the intensities of the signals for $[Au_1]^+$, $[Au_2]^+$, and $[Au_3]^+$ species decreased to 59.3, 65.3, and 68.0%, respectively, of their corresponding signals in Figure 2C. Fibrinogen possesses three nonidentical polypeptide chains (Aα, Bβ, γ) linked together by 29 disulfide bonds and form two distal D regions, one central E region, and two αC regions to form a 45 nm-long dimer plasma glycoprotein (340 kDa).[47] When thrombin cleaves the two fibrinopeptides A and B in the fibrinogen during the fibrinogen assembly process (binding knobs "A" and "B" in the central nodule of the fibrinogen monomer to complementary holes "a" and "b" in the α- and β-nodules), the monomers associate into two-stranded proto-fibrils, which then aggregate laterally to form the fibrin clot.[48] When we dipped a Au NPs–MCEM into a fibrinogen solution, the fibrinogen molecules self-adsorbed onto the Au NPs, presumably with a "side-on" (laying on the surface) orientation.[49] Once introduced into the solution containing the Au NPs–MCEM, thrombin-mediated polymerization of fibrinogen took place and insoluble fibrillar fibrin layer was formed on the MCEM (Figure 1d). As a result, the Au NPs absorbed less laser energy after laser excitation and transferred this energy to the surface fibrin layer; consequently, it suppressed the evaporation of Au atoms and thus decreased the Au cluster cations signals in the mass spectra (Figure 2D). In addition, the dense coverage of fibrin structures on the Au NPs–MCEM might have strongly inhibited electron ejection from the Au NPs and sharply decreased the Au NPs' electron temperature.[15−17] Therefore, explosive fragmentation was suppressed, inhibiting the formation of relatively large Au cluster ions.

Parameters for Au NP–MCEM in LDI–MS. We studied the effect of the particle size of the Au NPs in the fibrinogen/Au NPs–MCEM assembly on the detection of thrombin when monitoring the signals of the $[Au_1]^+$ ion. Figure S1B represents the TEM images of Au NPs, which clearly indicate the formation of 13, 32, and 56 nm Au NPs. The increase in the $[Au_2]^+$ and $[Au_3]^+$ signal strength in the LDI–MS with the increase in thrombin concentration was not linear and showed high RSD at lower concentrations. Hence, they do not show

significance in thrombin detection. Best results were obtained for thrombin detection (0−1.0 nM) when using 13 nm Au NPs (Figure S2, Supporting Information). The synthesized 13, 32, and 56 nm Au NPs were dispersed without aggregation on the MCEM as can be seen from Figure S3A (Supporting Information). The signal intensity of $[Au_1]^+$ ions from the Au NPs−MCEM under pulse irradiation (5.57×10^4 W cm^{-2}) decreased with increase in the Au NPs size, probably due to the easy fragmentation of smaller Au NPs. In addition, the 13 nm Au NPs were split almost completely from the MCEM after laser irradiation, unlike the 32 and 56 nm Au NPs (Figure S3B). The 13 nm Au NPs absorbed laser energy and easily split off from the MCEM when their temperature was above the boiling point (ca. 3000 K) or the value of T_e^{frag} (electron ejection−induced fragmentation at ca. 8000 K).[11] Notably, NPs of noble metals exhibit a decrease in boiling point upon decreasing the particle size. Instead of size reduction or fragmentation, we observed that some of the 32 and 56 nm Au NPs fused to form larger particles (60−150 nm) after pulse irradiation on the MCEM (Figure S3B). For a nanosecond laser pulse, the thermal effect dominates the melting and fusion of the Au NPs because the thermal coupling time between electrons and the lattice laser pulse (ca. 1 ps) are much shorter than the duration of the laser pulse.[3,11] In such a case, the whole Au NP will be heated. At a threshold temperature, the whole Au NP will melt and adjacent NPs can fuse to form perfectly spherical NPs.

Next, we investigated the influence of laser power density on detection of thrombin using the MCEM modified with 13 nm Au NPs. The laser power density strongly influenced the surface melting and evaporation of Au NPs; however, the excitation wavelength of laser did not affect much.[15,27,29] Figure S4B (Supporting Information) indicates that a laser power density of 5.57×10^4 W cm^{-2} was optimum for the analysis of thrombin. The lattice temperature and electron temperature of Au NPs increase upon increasing the laser power density; as a result, the signal intensities of the $[Au_1]^+$ ions increased as the laser density increased from 5.24×10^4 to 6.24×10^4 W cm^{-2} (Figure S4A, Supporting Information). Although a lower mass spectral background (noise) was generated at a lower power density (<5.24×10^4 W cm^{-2}), the energy was insufficient to produce the required ionization efficiency. At higher power densities, however, complicated mass spectra were obtained due to the formation of Au cluster ion adducts and fragmentation and ionization of surface molecules. Notably, laser irradiation at relatively high intensities (>5.57×10^4 W cm^{-2}; Figure S5, Supporting Information) not only induced the fragmentation, splitting, and/or fusion of the Au NPs on the MCEM but also formed large (ca. 1−5 μm) craters on the MCEM surface. We also observed such craters on the fibrin-adsorbed MCEM (Figure S6, Supporting Information). Thus, the formation of $[Au_n]^+$ cluster ions was not sensitive to the surface properties of the MCEM under a too-high laser power density because the laser irradiation could also induce the splitting and fragmentation of interior Au NPs. To avoid high background noise, loss in resolution, and serious destruction of the MCEM substrates, we chose a value of 5.57×10^4 W cm^{-2} for our following experiments.

Selectivity and Practicality. Thrombin is an important biomarker for a variety of health problems such as coagulation abnormalities, metastasis, tumors, and angiogenesis.[36,37] The challenge in quantitative detection of thrombin is its varying concentration in blood; for example, the free thrombin concentration can vary from nanomolar to micromolar during a coagulation reaction. However, under normal conditions, thrombin is absent in the blood. Patients with high-picomolar level of thrombin in their blood are prone to coagulation disorders. Thus, development of a rapid detection method that can detect picomolar concentrations of thrombin in plasma is indispensable. Under the optimal laser power (5.57×10^4 W cm^{-2}), we evaluated the selectivity and sensitivity of our Fib−Au NPs−MCEM/LDI−MS system for the analysis of thrombin. First, we tested the specificity of the Fib−Au NPs−MCEM probe (Figure 3) for the analysis of various

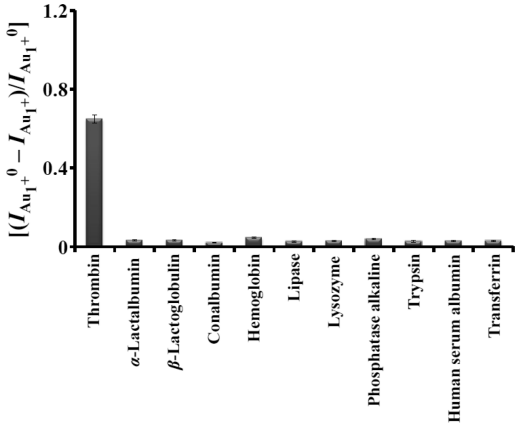

Figure 3. Selectivity test of the Fib−Au NPs−MCEM substrate combined with LDI−MS for various proteins and enzymes in PBS containing 100 μM BSA. The concentrations of thrombin and other proteins/enzymes were 100 pM and 10 nM, respectively. $I_{Au1+}{}^0$ and I_{Au1+} represent the signal intensities of $[Au_1]^+$ ions in the absence and presence of protein/enzyme, respectively. Error bars represent standard deviations from five repeated experiments. Other conditions were the same as those described in Figure 1.

proteins and enzymes (thrombin, α-lactalbumin, β-lactoglobulin, conalbumin, hemoglobin, lipase, lysozyme, phosphatase alkaline, trypsin, human serum albumin, and transferrin; the concentration of thrombin and each of other proteins was 100 pM and 10 nM, respectively) in the presence of backgroud protein, BSA (100 μM). Our system showed 1000-fold selectivity or more toward thrombin over the other proteins and enzymes. We also noted only thrombin-mediated formation of fibrin layer on Au NPs−MCEM from the SEM measurements (data not shown). The tolerance concentrations of the other proteins or enzymes were at least 1000 times greater than the thrombin concentration with the detection of 100 pM thrombin (within a relative error range of ±10%; data not shown). Figure 4 reveals that our Fib−Au NPs−MCEM probe could selectively detect thrombin with a limit of detection (LOD) of 2.5 pM (ca. 9.35×10^{-5} NIH units) in 10-fold-diluted plasma samples. These results demonstrate the practicality of using Fib−Au NPs−MCEM probe for monitoring thrombin gerneration. Compared to other NP-based sensors for thrombin detection,[50−54] our label-free assay is relatively rapid and has good sensitivity. Notably, most other NP-based sensors require covalent conjugation of aptamers, fluorophores, and electroactive species to the NPs.[50−54] Moreover, most optical and electrochemical probes based on NPs are seldom empolyed for quantitative detection of thrombin in biological samples such as plasma. Unlike other probes which generally determine the concentration of

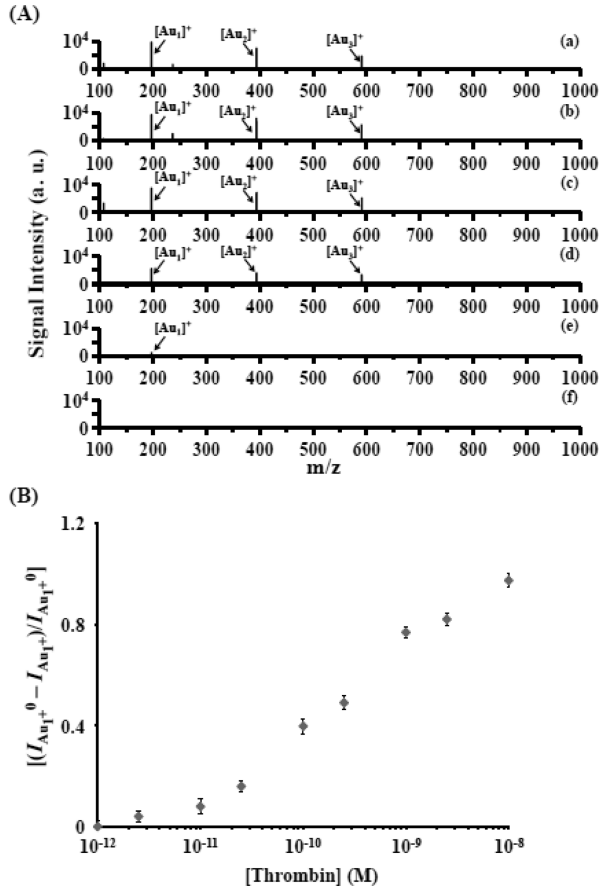

Figure 4. (A) Mass spectra recorded for Fib–Au NPs–MCEM as a probe for the detection of (a) 0 pM, (b) 2.5 pM, (c) 10 pM, (d) 100 pM, (e) 1 nM, and (f) 10 nM thrombin spiked in a 10-fold-diluted plasma sample. (B) Relative signal intensities of $[Au_1]^+$ ions $[(I_{Au1+}{}^0 - I_{Au1+})/I_{Au1+}{}^0]$ plotted with respect to the concentration of thrombin (0–10 nM). $I_{Au1+}{}^0$ and I_{Au1+} represent the signal intensities of $[Au_1]^+$ ions in the absence and presence, respectively, of thrombin. Other conditions were the same as those described in Figure 1.

thrombin,[50−54] our assay determines the activity of thrombin; note that the function of blood coagulation is highly related to the activity of thrombin, rather than its concentration.

We further applied our Fib–Au NPs–MCEM probe to monitor TG in plasma triggered by activated Factor X (Factor Xa; activated by both factors IX and VII with its cofactor, tissue factor). Thrombin is produced through the Factor Xa-mediated enzymatic cleavage of two sites on prothrombin. Assembly of the prothrombinase complex (Factor Va–Factor Xa) can result in a 300 000-fold increase in the rate of prothrombin conversion.[55] Many anticoagulants have been developed with targeted action against Factor Xa or thrombin.[56−58] Before analysis using our developed assay, we prepared representative 200-fold diluted plasma samples in saline buffer spiked with Factor Xa (final concentrations: 0–10 pM). The dose–response curve obtained revealed that our Fib–Au NPs–MCEM/LDI–MS system could detect Factor Xa in plasma samples at concentrations down to 0.5 pM (Figure S7, Supporting Information), suggesting that our probing system should be useful for monitoring TG in plasma under physiological conditions.

Inhibition Assays of Thrombin. The exosites I and II of thrombin that are located adjacent to the active site provide its proteolytic activity with specificity by facilitating binding of the inhibitors with the substrates.[59−61] Figure 5 reveals that the Fib–Au NPs–MCEM/LDI–MS system could be used to

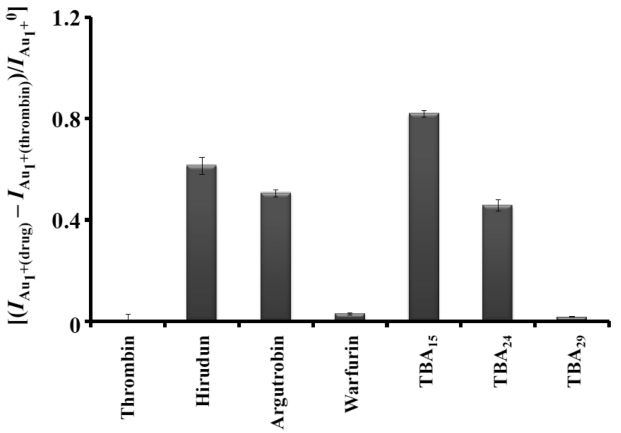

Figure 5. Validation of the use of the Fib–Au NPs–MCEM/LDI–MS system to screen inhibitors of thrombin. Relative signal intensities of $[Au_1]^+$ ions $[(I_{Au1+(drug)} - I_{Au1+(thrombin)})/I_{Au1+}{}^0]$, where $I_{Au1+(drug)}$ is the signal intensity of $[Au_1]^+$ ions in the presence of 1.0 nM thrombin and 1.0 μM drug or 100 nM TBA; $I_{Au1+(thrombin)}$ is the signal intensity of $[Au_1]^+$ ions in the presence of 1.0 nM thrombin, but in the absence of a drug or TBA; and $I_{Au1+}{}^0$ is the $[Au_1]^+$ signal intensity of the Fib–Au NPs–MCEM alone. Error bars represent standard deviations from three repeated experiments. Other conditions were the same as those described in Figure 4.

investigate the inhibition reactions of direct thrombin inhibitors (DTIs) and thrombin. We studied the three best-known thrombin-binding aptamers (TBAs): 29-base-long aptamer (TBA_{29}), which binds with exosite II, and 15-base-long aptamer (TBA_{15}) and 24-base-long aptamer (TBA_{24}), which interact to exosite I, with dissociation constants (K_d) of approximately 0.5, 100, and 10 nM, respectively.[62−65] For use as potential anticoagulants, only TBA_{15} and TBA_{24} possess enzymatic inhibitory functions to thrombin-mediated coagulation, because these two aptamers bind with the fibrinogen-binding exosite I.[65] We observed that the thrombin activity (1.0 nM) was inhibited to approximately 95% by TBA_{15} (100 nM) and to approximately 60% by TBA_{24} (100 nM), whereas TBA_{29} (100 nM) exhibited no obvious anticoagulant activity. We also noted that hirudin, a 65-amino-acid polypeptide suppressed thrombin activity to ca. 75% by simultaneously interacting with both exosite I and active site with ultrahigh affinity (K_d = ca. 10^{-14} M).[66] Results from our assay also agree with the previous observation that argatroban can act as a DTI and inhibits thrombin activity by binding to the active site of thrombin reversibly, without the need for the cofactor AT III for inhibition,[67,68] whereas warfarin is not a DTI. Warfarin, a coumarin derivative, works by suppressing the production of some clotting factors (II, VII, IX, X).[69,70] Warfarin also interferes with the synthesis of anticoagulant factors, protein C, protein S, and protein Z.[70] Taken together, our results suggest that the Fib–Au NPs–MCEM/LDI–MS system can be potentially applied for rapid screening of DTIs as anticoagulant drugs.

CONCLUSIONS

We have demonstrated that the formation of fibrin from fibrinogen through the action of thrombin can be monitored using Au NPs–MCEMs coupled with LDI–MS. The fibrin

formed on the Au NPs−MCEM significantly inhibited the formation and desorption of Au cluster ions during the laser-induced desorption and ionization processes in the LDI−MS analysis. The size of the Au NPs and the laser intensity both greatly affected the formation and desorption of cationic Au clusters, as well as the fusion of the Au NPs to form larger particles, because the thermal coupling time between electrons and lattice was remarkably shorter than the duration of the laser pulses. The diminished peak intensities of Au cluster ions was caused by the fibrin that formed on the surfaces of the Au NPs that absorbed energy from them and suppressed the evaporation of Au atoms. We successfully demonstrated the application of this membrane-based probe for monitoring TG and Factor Xa in human plasma down to the picomolar regime. Furthermore, our probe displayed very good performance in monitoring the performance of DTIs in thrombin inhibition reactions. Because our probe can be employed to monitor a wide range of reactions, including TG, DTI-mediated inhibition of thrombin, and determination of the activity of Factor Xa under clinical conditions, this technique can be applied for diagnosing diseases associated with hemarthrosis, nose bleeding, and hematuria. Furthermore, the inhibition of the formation of Au cluster ions may be applied to the design of new assays for DNA, proteins, pathogens, and cancer cells and for the development of highly sensitive biosensors.

■ ASSOCIATED CONTENT

Supporting Information

Figures S1−S7, which represents the TEM of different sized Au NPs, SEM images of the Au NPs−MCEMs, the effect of laser density on the LDI−MS analysis, and the detection of Factor Xa spiked in plasma samples. This material is available free of charge via the Internet at http://pubs.acs.org.

■ AUTHOR INFORMATION

Corresponding Author

*Address: Institute of Bioscience and Biotechnology, National Taiwan Ocean University, 2, Beining Road, Keelung 20224, Taiwan. Tel.: 011-886-2-2462-2192, ext. 5517. Fax: 011-886-2-2462-2034. E-mail: huanging@ntou.edu.tw.

Notes

The authors declare no competing financial interest.

■ ACKNOWLEDGMENTS

This study was supported by the Ministry of Science and Technology of Taiwan under contract NSC 101-2628-M-019-001-MY3, 102-2113-M-019-001-MY3, and 102-2627-M-019-001-MY3.

■ REFERENCES

(1) Pyatenk, A.; Wang, H.; Koshizaki, N.; Tsuji, T. Mechanism of Pulse Laser Interaction with Colloidal Nanoparticles. *Laser Photon. Rev.* **2013**, *7*, 596−604.

(2) Singh, S. C.; Zeng, H. Nanomaterials and Nanopatterns Based on Laser Processing: A Brief Review on Current State of Art. *Sci. Adv. Mater.* **2012**, *4*, 368−390.

(3) Hashimoto, S.; Werner, D.; Uwada, T. Studies on the Interaction of Pulsed Lasers with Plasmonic Gold Nanoparticles toward Light Manipulation, Heat Management, and Nanofabrication. *J. Photochem. Photobiol., C* **2012**, *13*, 28−54.

(4) Pocoví-Martínez, S.; Parreño-Romero, M.; Agouram, S.; Pérez-Prieto, J. Controlled UV−C Light-Induced Fusion of Thiol-Passivated Gold Nanoparticles. *Langmuir* **2011**, *27*, 5234−5241.

(5) Stratakis, E. Nanomaterials by Ultrafast Laser Processing of Surfaces. *Sci. Adv. Mater.* **2012**, *4*, 407−431.

(6) Tan, D.; Zhou, S.; Qiu, J.; Khusro, N. Preparation of Functional Nanomaterials with Femtosecond Laser Ablation in Solution. *J. Photochem. Photobiol., C* **2013**, *17*, 50−68.

(7) Peláez, R. J.; Baraldi, G.; Afonso, C. N.; Riedel, S.; Boneberg, J.; Leiderer, P. Selective Gold Nanoparticles Formation by Pulsed Laser Interference. *Appl. Surf. Sci.* **2012**, *258*, 9223−9227.

(8) Zeng, H.; Du, X.-W.; Singh, S. C.; Kulinich, S. A.; Yang, S.; He, J.; Cai, W. Nanomaterials via Laser Ablation/Irradiation in Liquid: A Review. *Adv. Funct. Mater.* **2012**, *22*, 1333−1353.

(9) Giammanco, F.; Giorgetti, E.; Marsili, P.; Giusti, A. Experimental and Theoretical Analysis of Photofragmentation of Au Nanoparticles by Picosecond Laser Radiation. *J. Phys. Chem. C* **2010**, *114*, 3354−3363.

(10) Akman, E.; Aktas, O. C.; Genc Oztoprak, B.; Gunes, M.; Kacar, E.; Gundogdu, O.; Demir, A. Fragmentation of the Gold Nanoparticles Using Femtosecond Ti:Sapphire Laser and Their Structural Evolution. *Opt. Laser Technol.* **2013**, *49*, 156−160.

(11) Werner, D.; Hashimoto, S. Improved Working Model for Interpreting the Excitation Wavelength- and Fluence-Dependent Response in Pulsed Laser-Induced Size Reduction of Aqueous Gold Nanoparticles. *J. Phys. Chem. C* **2011**, *115*, 5063−5072.

(12) Shoji, M.; Miyajima, K.; Mafuné, F. Ionization of Gold Nanoparticles in Solution by Pulse Laser Excitation as Studied by Mass Spectrometric Detection of Gold Cluster Ions. *J. Phys. Chem. C* **2008**, *112*, 1929−1932.

(13) Akchurin, G.; Khlebtsov, B.; Akchurin, G.; Tuchin, V.; Zharov, V.; Khlebtsov, N. Gold Nanoshell Photomodification under A Single-Nanosecond Laser Pulse Accompanied by Color-Shifting and Bubble Formation Phenomena. *Nanotechnology* **2008**, *19*, 015701.

(14) Zedan, A. F.; Moussa, S.; Terner, J.; Atkinson, G.; El-Shall, M. S. Ultrasmall Gold Nanoparticles Anchored to Graphene and Enhanced Photothermal Effects by Laser Irradiation of Gold Nanostructures in Graphene Oxide Solutions. *ACS Nano* **2013**, *7*, 627−636.

(15) Werner, D.; Furube, A.; Okamoto, T.; Hashimoto, S. Femtosecond Laser-Induced Size Reduction of Aqueous Gold Nanoparticles: In Situ and Pump−Probe Spectroscopy Investigations Revealing Coulomb Explosion. *J. Phys. Chem. C* **2011**, *115*, 8503−8512.

(16) Muto, H.; Miyajima, K.; Mafuné, F. Mechanism of Laser-Induced Size Reduction of Gold Nanoparticles as Studied by Single and Double Laser Pulse Excitation. *J. Phys. Chem. C* **2008**, *112*, 5810−5815.

(17) Miyasaka, Y.; Hashida, M.; Ikuta, Y.; Otani, K.; Tokita, S.; Sakabe, S. Nonthermal Emission of Energetic Ions from A Metal Surface Irradiated by Extremely Low-Fluence Femtosecond Laser Pulses. *Phys. Rev. B* **2012**, *86*, 075431.

(18) Kim, S. J.; Jang, D.-J. Laser-Induced Nanowelding of Gold Nanoparticles. *Appl. Phys. Lett.* **2005**, *86*, 033112.

(19) Saha, K.; Agasti, S. S.; Kim, C.; Li, X.; Rotello, V. M. Gold Nanoparticles in Chemical and Biological Sensing. *Chem. Rev.* **2012**, *112*, 2739−2779.

(20) Dykman, L.; Khlebtsov, N. Gold Nanoparticles in Biomedical Applications: Recent Advances and Perspectives. *Chem. Soc. Rev.* **2012**, *41*, 2256−2282.

(21) Jans, H.; Huo, Q. Gold Nanoparticle-Enabled Biological and Chemical Detection and Analysis. *Chem. Soc. Rev.* **2012**, *41*, 2849−2866.

(22) Zhu, S.; Chen, T. P.; Liu, Y. C.; Liu, Y.; Fung, S. A Quantitative Modeling of the Contributions of Localized Surface Plasmon Resonance and Interband Transitions to Absorbance of Gold Nanoparticles. *J. Nanopart. Res.* **2012**, *14*, 856.

(23) Myroshnychenko, V.; Rodríguez-Fernández, J.; Pastoriza-Santos, I.; Funston, A. M.; Novo, C.; Mulvaney, P.; Liz-Marzán, L. M.; García de Abajo, F. J. Modelling the Optical Response of Gold Nanoparticles. *Chem. Soc. Rev.* **2008**, *37*, 1792−1805.

(24) Ghosh, S. K.; Pal, T. Interparticle Coupling Effect on the Surface Plasmon Resonance of Gold Nanoparticles: From Theory to Applications. *Chem. Rev.* **2007**, *107*, 4797−4862.
(25) Zhu, J. Shift Fashion of Surface Plasmon Resonances in Non-Spherical Gold Nanoparticles: A Simple Model of Surface Plasmon Dynamics. *Curr. Nanosci.* **2013**, *5*, 216−219.
(26) Wysin, G. M.; Chikan, V.; Young, N.; Dani, R. K. Effects of Interband Transitions on Faraday Rotation in Metallic Nanoparticles. *J. Phys.: Condens. Matter* **2013**, *25*, 325302.
(27) Werner, D.; Hashimoto, S.; Uwada, T. Remarkable Photothermal Effect of Interband Excitation on Nanosecond Laser-Induced Reshaping and Size Reduction of Pseudospherical Gold Nanoparticles in Aqueous Solution. *Langmuir* **2010**, *26*, 9956−9963.
(28) Werner, D.; Hashimoto, S. Controlling the Pulsed-Laser-Induced Size Reduction of Au and Ag Nanoparticles via Changes in the External Pressure, Laser Intensity, and Excitation Wavelength. *Langmuir* **2013**, *29*, 1295−1302.
(29) Yamada, K.; Miyajima, K.; Mafuné, F. Thermionic Emission of Electrons from Gold Nanoparticles by Nanosecond Pulse-Laser Excitation of Interband. *J. Phys. Chem. C* **2007**, *111*, 11246−11251.
(30) Yamada, K.; Tokumoto, Y.; Nagata, T.; Mafuné, F. Mechanism of Laser-induced Size-reduction of Gold Nanoparticles as Studied by Nanosecond Transient Absorption Spectroscopy. *J. Phys. Chem. B* **2006**, *110*, 11751−11756.
(31) Liu, Y.-C.; Li, Y.-J.; Huang, C.-C. Information Derived from Cluster Ions from DNA-Modified Gold Nanoparticles under Laser Desorption/Ionization: Analysis of Coverage, Structure, and Single-Nucleotide Polymorphism. *Anal. Chem.* **2013**, *85*, 1021−1028.
(32) Liu, Y.-C.; Chiang, C.-K.; Chang, H.-T.; Lee, Y.-F.; Huang, C.-C. Using a Functional Nanogold Membrane Coupled with Laser Desorption/Ionization Mass Spectrometry to Detect Lead Ions in Biofluids. *Adv. Funct. Mater.* **2011**, *21*, 4448−4455.
(33) Liu, Y.-C.; Chang, H.-T.; Chiang, C.-K.; Huang, C.-C. Pulsed-Laser Desorption/Ionization of Clusters from Biofunctional Gold Nanoparticles: Implications for Protein Detections. *ACS Appl. Mater. Interfaces* **2012**, *4*, 5241−5248.
(34) Qi, D. W.; Zhang, H. Y.; Tang, J.; Deng, C. H.; Zhang, X. M. Facile Synthesis of Mercaptophenylboronic Acid-Functionalized Core−Shell Structure Fe_3O_4@C@Au Magnetic Microspheres for Selective Enrichment of Glycopeptides and Glycoproteins. *J. Phys. Chem. C* **2010**, *114*, 9221−9226.
(35) Hu, J. J.; Ma, R. N.; Liu, F.; Chen, Y. L.; Ju, H. X. Mercaptophenylboronic Acid Modified Gold Nanoparticle@silica Bubbles for Buoyant Separation and Specific Enrichment of Glycopeptides. *RSC Adv.* **2014**, *4*, 28856−28859.
(36) Tanaka, K. A.; Key, N. S.; Levy, J. H. Blood Coagulation: Hemostasis and Thrombin Regulation. *Anesth. Analg.* **2009**, *108*, 1433−1446.
(37) Di Cera, E. Thrombin. *Mol. Asp. Med.* **2008**, *29*, 203−254.
(38) Campo, G.; Pavasini, P.; Pollina, A.; Fileti, L.; Marchesini, J.; Tebaldi, M.; Ferrari, R. Thrombin Generation Assay: A New Tool to Predict and Optimize Clinical Outcome in Cardiovascular Patients? *Blood Coagulation Fibrinolysis* **2012**, *23*, 680−687.
(39) ten Cate, H. Thrombin Generation in Clinical Conditions. *Thromb. Res.* **2012**, *129*, 367−370.
(40) Al Dieri, R.; de Laat, B.; Hemker, H. C. Thrombin Generation: What Have We Learned? *Blood Rev.* **2012**, *26*, 197−203.
(41) Chen, C.-K.; Huang, C.-C.; Chang, H.-T. Label-free colorimetric detection of picomolar thrombin in blood plasma using a gold nanoparticle-based assay. *Biosens. Bioelectron.* **2010**, *25*, 1922−1927.
(42) Turkevich, J. Colloidal Gold. Part II. *Gold Bull.* **1985**, *18*, 125−131.
(43) Chiu, W.-C.; Huang, C.-C. Combining Fibrinogen-Conjugated Gold Nanoparticles with a Cellulose Membrane for the Mass Spectrometry-Based Detection of Fibrinolytic-Related Proteins. *Anal. Chem.* **2013**, *85*, 6922−6929.
(44) Bisker, G.; Yelin, D. Noble-Metal Nanoparticles and Short Pulses for Nanomanipulations: Theoretical Analysis. *J. Opt. Soc. Am. B* **2012**, *29*, 1383−1393.
(45) King, B. V.; Veryovkin, I. V.; Moore, J. F.; Calaway, W. F.; Pellin, M. J. Formation of Neutral Clusters during Sputtering of Gold. *Surf. Sci.* **2009**, *603*, 819−825.
(46) Holle, A.; Haase, A.; Kayser, M.; Höhndorf, J. Optimizing UV Laser Focus Profiles for Improved MALDI Performance. *J. Mass Spectrom.* **2006**, *41*, 705−716.
(47) Brown, J. H.; Volkmann, N.; Jun, G.; Henschen-Edman, A. H.; Cohen, C. The Crystal Structure of Modified Bovine Fibrinogen. *Proc. Natl. Acad. Sci. U.S.A.* **2000**, *97*, 85−90.
(48) Weisel, J. W.; Litvinov, R. I. Mechanisms of Fibrin Polymerization and Clinical Implications. *Blood* **2013**, *121*, 1712−1719.
(49) Deng, Z. J.; Liang, M.; Toth, I.; Monteiro, M. J.; Minchin, R. F. Molecular Interaction of Poly(acrylic acid) Gold Nanoparticles with Human Fibrinogen. *ACS Nano* **2012**, *6*, 8962−8969.
(50) Jiang, Z.; Yang, T.; Liu, M.; Hu, Y.; Wang, J. An Aptamer-Based Biosensor for Sensitive Thrombin Detection with Phthalocyanine@SiO_2 Mesoporous Nanoparticles. *Biosens. Bioelectron.* **2014**, *53*, 340−345.
(51) Li, J.; Li, W.; Qiang, W.; Wang, X.; Li, H.; Xu, D. A Non-Aggregation Colorimetric Assay for Thrombin Based on Catalytic Properties of Silver Nanoparticles. *Anal. Chim. Acta* **2014**, *807*, 120−125.
(52) Li, W.; Qiang, W.; Li, J.; Li, H.; Dong, Y.; Zhao, Y.; Xu, D. Nanoparticle-Catalyzed Reductive Bleaching for Fabricating Turn-off and Enzyme-free Amplified Colorimetric Bioassays. *Biosens. Bioelectron.* **2014**, *51*, 219−224.
(53) Zhuo, Y.; Ma, M.-N.; Chai, Y.-Q.; Zhao, M.; Yuan, R. Amplified Electrochemiluminescent Aptasensor Using Mimicking Bi-Enzyme Nanocomplexes as Signal Enhancement. *Anal. Chim. Acta* **2014**, *809*, 47−53.
(54) Jiang, C.; Zhao, T.; Li, S.; Gao, N.; Xu, Q.-H. Highly Sensitive Two-Photon Sensing of Thrombin in Serum Using Aptamers and Silver Nanoparticles. *ACS Appl. Mater. Interfaces* **2013**, *5*, 10853−10857.
(55) Krishnaswamy, S. The Transition of Prothrombin to Thrombin. *J. Thromb. Haemostasis* **2013**, *11*, 265−276.
(56) van Montfoort, M. L.; Meijers, J. C. M. Anticoagulation beyond Direct Thrombin and Factor Xa Inhibitors: Indications for Targeting the Intrinsic Pathway? *Thromb. Haemostasis* **2013**, *110*, 223−232.
(57) Yates, S.; Sarode, R. Novel Thrombin and Factor Xa Inhibitors: Challenges to Reversal of Their Anticoagulation Effects. *Curr. Opin. Hematol.* **2013**, *20*, 552−557.
(58) Straub, A.; Roehrig, S.; Hillisch, A. Oral, Direct Thrombin and Factor Xa Inhibitors: The Replacement for Warfarin, Leeches, and Pig Intestines? *Angew. Chem., Int. Ed.* **2011**, *50*, 4574−4590.
(59) Nimjee, S. M.; Oney, S.; Volovyk, Z.; Bompiani, K. M.; Long, S. B.; Hoffman, M.; Sullenger, B. A. Synergistic Effect of Aptamers that Inhibit Exosites 1 and 2 on Thrombin. *RNA* **2009**, *15*, 2105−2111.
(60) Gandhi, P. S.; Chen, Z.; Appelbaum, E.; Zapata, F.; Di Cera, E. Structural Basis of Thrombin−Protease-Activated Receptor Interactions. *IUBMB Life* **2011**, *63*, 375−382.
(61) Petrera, N. S.; Stafford, A. R.; Leslie, B. A.; Kretz, C. A.; Fredenburgh, J. C.; Weitz, J. I. Long Range Communication between Exosites 1 and 2 Modulates Thrombin Function. *J. Biol. Chem.* **2009**, *284*, 25620−25629.
(62) Zavyalova, E.; Golovin, A.; Timoshenko, T.; Babiy, A.; Pavlova, G.; Kopylov, A. DNA Aptamers for Human Thrombin with High Anticoagulant Activity Demonstrate Target- and Species-Specificity. *Curr. Med. Chem.* **2013**, *19*, 5232−5237.
(63) Musumeci, D.; Montesarchio, D. Polyvalent Nucleic Acid Aptamers and Modulation of Their Activity: A Focus on the Thrombin Binding Aptamer. *Pharmacol. Ther.* **2012**, *136*, 202−215.
(64) Bock, L. C.; Griffin, L. C.; Latham, J. A.; Vermaas, E. H.; Toole, J. J. Selection of Single-Stranded DNA Molecules that Bind and Inhibit Human Thrombin. *Nature* **1992**, *355*, 564−566.
(65) Chen, Y.-Y.; Tseng, C.-W.; Chang, H.-Y.; Hung, Y.-L.; Huang, C.-C. Gold nanoparticle-based colorimetric assays for coagulation-related proteins and their inhibition reactions. *Biosens. Bioelectron.* **2011**, *26*, 3160−3166.

(66) Rydel, T. J.; Ravichandran, K. G.; Tulinsky, A.; Bode, W.; Huber, R.; Roitsch, C.; Fenton, J. W. The Structure of a Complex of Recombinant Hirudin and Human α-Thrombin. *Science* **1990**, *249*, 277−280.
(67) Escolar, G.; Bozzo, J.; Maragall, S. Argatroban: A Direct Thrombin Inhibitor with Reliable and Predictable Anticoagulant Actions. *Drugs Today* **2006**, *42*, 223.
(68) Serebruany, M. V.; Malinin, A. I.; Serebruany, V. L.; Argatroban, A. Direct Thrombin Inhibitor for Heparin-Induced Thrombocytopaenia: Present and Future Perspectives. *Expert Opin. Pharmacother.* **2006**, *7*, 81−89.
(69) Adam, S. S.; McDuffie, J. R.; Ortel, T. L.; Williams, J. W. Comparative Effectiveness of Warfarin and New Oral Anticoagulants for the Management of Atrial Fibrillation and Venous Thromboembolism. *Ann. Int. Med.* **2012**, *157*, 796−807.
(70) Daly, A. K. Optimal Dosing of Warfarin and Other Coumarin Anticoagulants: The Role of Genetic Polymorphisms. *Arch. Toxicol.* **2013**, *87*, 407−420.